

Characterization of the 40 m radiotelescope at 5, 6, 8 and 22 GHz

P. de Vicente

Informe Técnico IT-OAN 2010-10

Revision history

Version	Date	Author	Updates
1.0	10-03-2010	P. de Vicente	First version
1.1	03-05-2010	P. de Vicente	Final version
1.2	03-08-2010	P. de Vicente	Updates with X band horn at a new position which maximizes the gain

Contents

1	Introduction	3
2	Skydips: forward efficiency and atmospheric opacity	3
3	Gain curves	9
4	Apperture efficiency, beam efficiency and SEFD	14
5	Beam images	17
5.1	C Band	17
5.2	X Band	19
5.3	K Band	19
5.4	Discussion	19

1 Introduction

This report explains the methods followed to characterize the 40 m radiotelescope at the following frequencies: 5, 6, 8 and 22 GHz and the results obtained. All these works have been performed before the surface of the primary reflector was adjusted and therefore results correspond to the status of the telescope between June 2008 and July 2010. Some of the results presented here suggest that a deeper study should be performed on some areas. In particular it is convenient to understand why the gain changes as a function of elevation in a different way at low and high (22 GHz) frequencies. Further studies should also be performed on skydips and on the role of the vertex membrane on the attenuation of the signal at different frequencies. All these studies are pending until panels in the main reflector are set according to holographic measurements.

2 Skydips: forward efficiency and atmospheric opacity

Skydips are drifts on the sky performed from horizon to zenith (5 to 89 degrees) usually done in regular steps. They are a measurement of the sky emissivity at different elevations and its coupling to the antenna. Skydips allow to determine the atmospheric opacity and the antenna forward efficiency.

The antenna sky temperature can be written as:

$$T_{sky}^a = \eta_f T_{atm} (1 - e^{-\tau_0 A}) + T_{rx} + T_g (1 - \eta_f) \quad (1)$$

where η_f is the forward efficiency and represents the fraction of radiation that enters the horn from the front part of the antenna. T_{atm} is the atmospheric temperature and, as an approximation, can be considered to be the ground temperature minus 40 degrees. τ_0 is the atmospheric opacity in the zenith and A the number of airmasses (1 towards the zenith). T_{rx} is the receiver temperature and T_g the ground temperature.

Some of these variables, like T_g and T_{rx} , are measured independently, and T_{atm} is always estimated from the ground temperature. The opacity can be estimated as a first guess from applications which use a standard atmospheric model for the northern hemisphere at mid latitudes. We have tested ATM (Pardo 2001) and AM (Paine 2004). These programs use a multilayer atmosphere model plus weather conditions at the surface or the amount of precipitable water in the nearby of the observatory. Both models take into account contributions from dry air (N_2 , O_2 , O_3) and H_2O .

The dependence of the antenna temperature with elevation comes from the product $\tau_0 A$ and therefore it is possible to obtain the opacity by fitting the data with a curve like the one in expression 1. The forward efficiency is also obtained from the same fit, since it has a big influence on the flat tail of the curve at high elevations and on the tilt of the curve elsewhere.

The zenith opacity is dependent on the weather conditions, strongly at high frequencies and weakly at low frequencies and therefore also depends on the observing frequency. The forward efficiency can be considered independent of elevation, but depends on the frequency since the surface error increases with frequency and the illumination also depends on the frequency.

The airmass has been calculated using a planar atmosphere. This approximation gets worse with low elevations and overestimates the total opacity at such elevations. The airmass A is defined as:

$$A = \frac{1}{\cos(z)} = \frac{1}{\sin(el)} \quad (2)$$

where z is the zenithal angle and el the elevation.

A better approximation for the airmass taking into account the curvature of the Earth is, according to Rozenberg (1966):

$$A' = \frac{1}{\cos(z) + 0.025e^{-11 \cos(z)}} \quad (3)$$

Both models can be compared by examining Fig. 1. Differences are important for elevations lower than 10 degrees. At 10 degrees elevation, both formulas differ 0.12 airmasses and their ratio is 0.99 for a zenithal opacity of $\tau_0 = 0.06$.

$$e^{-\tau_0 A(10)} = e^{-\tau_0 / \sin(10^\circ)} = 0.713 \quad (4)$$

$$e^{-\tau_0 A'(10)} = e^{-\frac{\tau_0}{\sin(10^\circ) + 0.025e^{-11 \sin(10^\circ)}}} = 0.708 \quad (5)$$

Since radio observations with the 40m are seldom performed below 10 degrees, and the planar atmosphere approximation is simpler, from now on we will use it for computing the atmospheric opacity at any elevation.

Forward efficiency for Nasmyth telescopes may include effects from mirrors in the cabin. These mirrors can pick up radiation from the cabin and be summed to the diffraction at the main dish borders, legs and subreflector which pick up radiation from the ground. The main difference is that the cabin temperature is usually at a constant temperature of 20 C and the ground temperature may be colder, similar or hotter, than this value by 30 degrees at most. In any case the value estimated here is a lower limit to the forward efficiency from the antenna, including the Nasmyth mirrors.

The atmospheric opacity can be computed from the precipitable water content in the atmosphere using applications like those mentioned above like ATM and AM. The amount of precipitable water can be roughly estimated from weather conditions in the surface. We will make some estimates that will allow us to check if the opacity values obtained from skydips match those from the local weather conditions. Most part of the derivation below is shown in Butler (1998).

The mass of precipitable water (m_{lw}) in the atmosphere can be written as:

$$m_{lw} = \rho_l A h \quad (6)$$

where ρ_l is the density of liquid water, A is the section of a column in the atmosphere, and h the height of the water column.

On the other hand the water column can be estimated by integrating the number of molecules along a column through the atmosphere. Let m_{wv} the mass of water vapour:

$$m_{wv} = A m_{H_2O} \int_0^\infty n_{wv} dZ \quad (7)$$

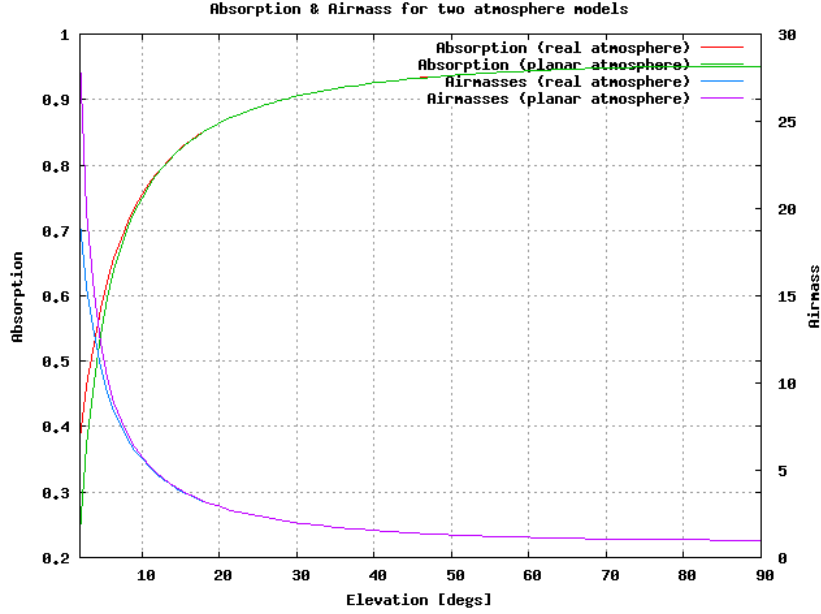


Figure 1: Predicted airmass and absorption due to a planar atmosphere and an approximation that takes into account the curvature of the Earth. Absorption was computed for a zenithal opacity of 0.06 (roughly the opacity at 22 GHz in winter under good conditions)

where m_{wv} is the mass of water vapour column of section A , m_{H_2O} the mass of a molecule of water (18 uam) and n_{wv} the density number of water vapour molecules. Z is a linear variable, height, along the atmosphere of Earth. The density number of molecules of water vapor may be considered to follow an exponential distribution as a function of height:

$$n_{wv} = n_s e^{(Z-Z_s)/H}$$

where n_s is the number of water vapour molecules at the surface of the Earth, Z_s the height of the observatory and H is a scale factor that indicates the height at which the column of water is 0.37 times that at the local surface. According to Ulich (1980) the scale is between 1500 and 2000 m.

Integrating we get:

$$n_{wv} = A m_{H_2O} n_s H$$

We can now equal equations 6 and 7 and we get:

$$\rho_l A h = A m_{H_2O} n_s H$$

The column of precipitable water is:

$$h = \frac{m_{H_2O} n_s H}{\rho_l}$$

According to the law of perfect gases:

$$n_s = \frac{P_{H_2O}}{K T_s}$$

where K is the Boltzmann constant and T_s the temperature in Kelvin at the surface of the Earth in the observatory. The partial pressure of water, P_{H_2O} in mbar can be written as a function of the dew temperature, T_d (Clark 1987):

$$P_{H_2O} = e^{1.81+17.27T_d/(T_d+237.3)}$$

The dew point is the temperature to which the air must be cooled, at barometric pressure, for the water vapour to condense into water. There are several approximations which give correct values between 0 and 60 degrees celsius. Below we show one:

$$T_d = (hr/100)^{1/8} (110 + T) - 110$$

where hr is the relative humidity and T the local temperature in degrees celsius. That is, $T_s = T + 273.16$

Hence the column of precipitable water vapour depends on a scale factor in meters for the water vapour presence in the atmosphere, the relative humidity and the surface atmospheric temperature:

$$h = \frac{e^{1.81+17.27T_d/(T_d+237.3)} m_{H_2O}}{\rho_l K T_s} H$$

We have assumed that the scale factor is 2 km. For practical purposes, and after replacing the values of each parameter in the proper units, the column of precipitable water in mm may be written as:

$$\begin{aligned} h[mm] &= \frac{10^2 e^{1.81+17.27T_d/(T_d+237.3)} 1.66053886 \cdot 10^{-27} 18}{10^3 1.3806503 \cdot 10^{-23} T_s} H \\ &= 432.98 \frac{e^{1.81+17.27T_d/(T_d+237.3)}}{T_s} \end{aligned}$$

The precipitable water in winter for a temperature of -2 C and a relative humidity of 77% is 5.9 mm whereas for summer ($T = 33$ C and relative humidity of 20%) it is 14 mm. However these conditions may vary from day to day and, in some cases, in the same day. The worst conditions in summer seem to happen at sunrise, for example $T = 18$ C and a relative humidity of 65%, correspond to 20 mm of precipitable water.

Atmospheric opacities at any frequency can be derived from these values and compared with the values obtained from skydips. Since the scale factor and some expression above are approximations, the values we obtain for precipitable water and, hence, opacity should be considered an estimation that allow to check if the results from the skydips match them.

Fits from skydips at C band (Fig. 2), frequencies between 4.9 and 6.6 GHz, require opacities between 0.009 and 0.012 and a forward efficiency of 0.89. Opacities are slightly larger and

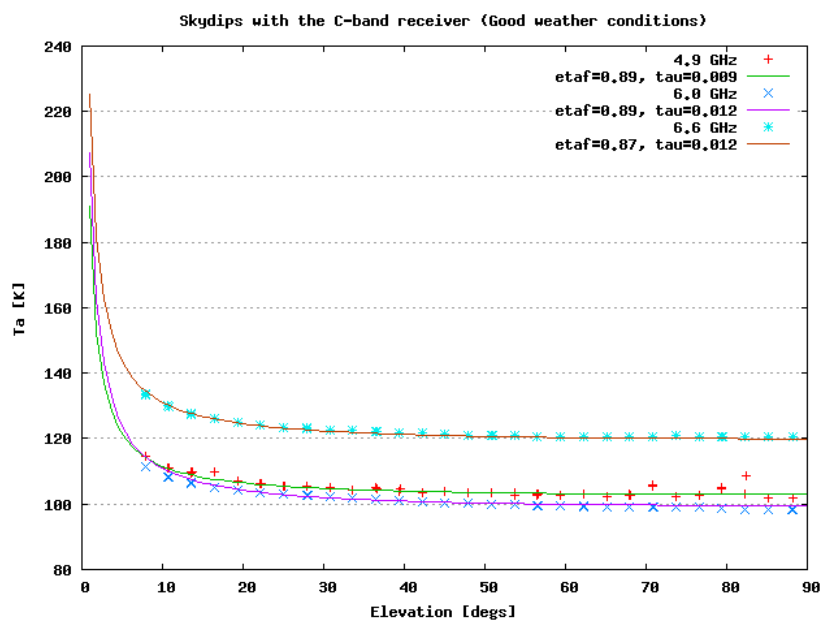


Figure 2: Skydips at 4.9 GHz, 6 and 6.6 GHz under good weather conditions: clear sky, pressure 902.9 mbar, humidity 60 % and temperature 0.3 C.

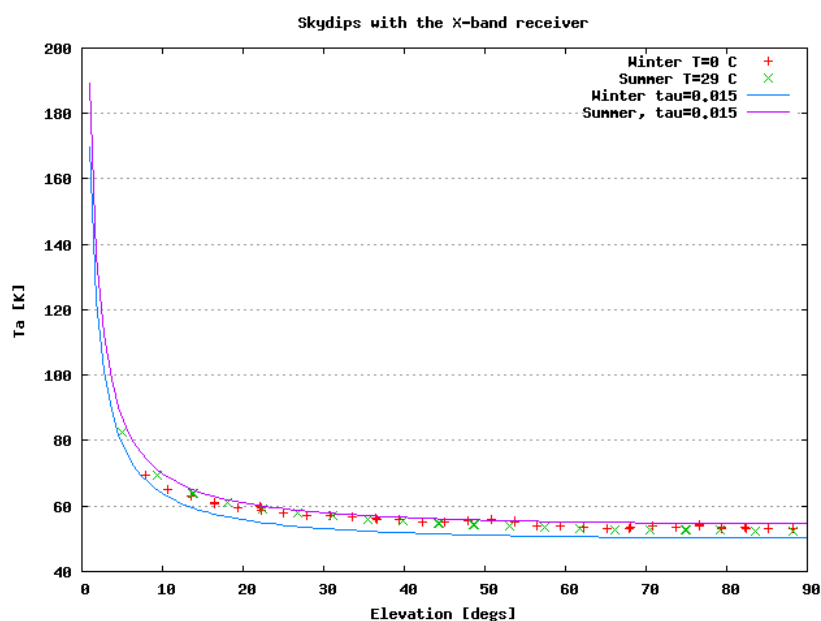


Figure 3: Skydips at 8 GHz in winter and summer. In both cases the sky was clear. Winter: pressure 905.7 mbar, humidity 49 % and temperature -0.1 C, Summer: pressure: 909 mbar, humidity 25 % and temperature 29 C. Forward efficiency is 0.85 and opacity 0.015 in both cases.

more disperse than 0.007 ± 0.0005 estimated by ATM for the whole interval from the ammount of precipitable water. There is an odd behaviour for the skydip at 6 GHz: the sky antenna temperature is better than at 4.9 GHz by ~ 5 K and better than at 6.6 GHz by ~ 20 K, whereas we expect values between 4.9 and 6.6 GHz if the receiver temperature is approximately the same.

The simplest explanation for this difference is to assume that the receiver temperature is better at 6 GHz. We have estimated that the receiver temperature should be, in that case, 67 K at 6 GHz. However the receiver temperature measured at the lab is 75 K. Another explanation is to assume that noise diode used for amplitude calibration is not properly calibrated or has some variable behaviour which impacts the skydips results.

In any case the opacity is so low at C band that the atmosphere has a negligible influence on the radiation at this frequency.

The skydip fits at 8 GHz (Fig. 3) predict an opacity of 0.015 both in winter and summer and a forward efficiency of 0.85. ATM estimates an opacity of 0.008 for a column of precipitable water of 8 mm and 12 mm.

The dependence of opacity on the atmospheric water content at this frequency is very weak. The forward efficiency is slightly lower than at C band. We believe that such a low value may be influenced by the nasmyth mirrors; in particular the dichroic mirror in front of the horn may contribute strongly to this figure. Skydips at 8.4 GHz with the same atmospheric conditions should be repeated by exchanging the dichroic mirror by a total reflection mirror to compare the results.

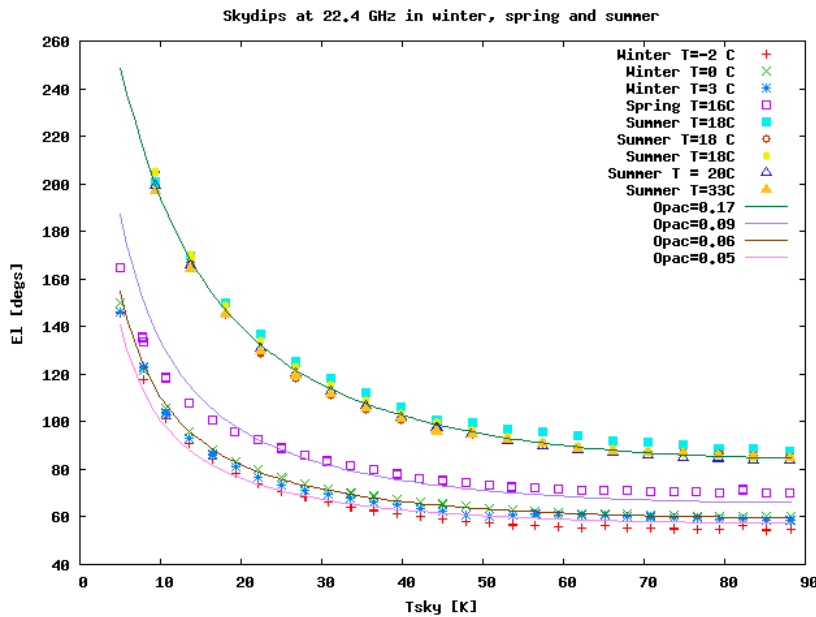


Figure 4: Skydips at 22.4 GHz under several weather conditions along the year. Lowest opacity happens in winter (0.06) and higher (0.17) in summer. The forward efficiency is $\eta_f = 0.93$ and has been computed using all curves.

We have also performed some skydips at 22.4 and 23.7 GHz under different atmospheric

conditions (Figs. 4 and 5). The atmosphere plays a very important role at this frequency due to the presence of the rotational line of water: 6(1,6)-5(2,3). Opacity may vary by a factor 3 in different seasons of the year. Different skydip curves allow to constrain the forward efficiency since it is independent of weather conditions. According to the skydip fits, forward efficiency is 0.93 ± 0.1 and the opacity varies from 0.06 in good winter conditions to 0.18 in summer conditions. ATM predicts these values for precipitable water columns of 8 and 25 mm respectively. In some cases variations of relative humidity within the same day do not seem to have an influence on opacity as obtained from skydips whereas in other cases like the one depicted in Fig. 5 they have.

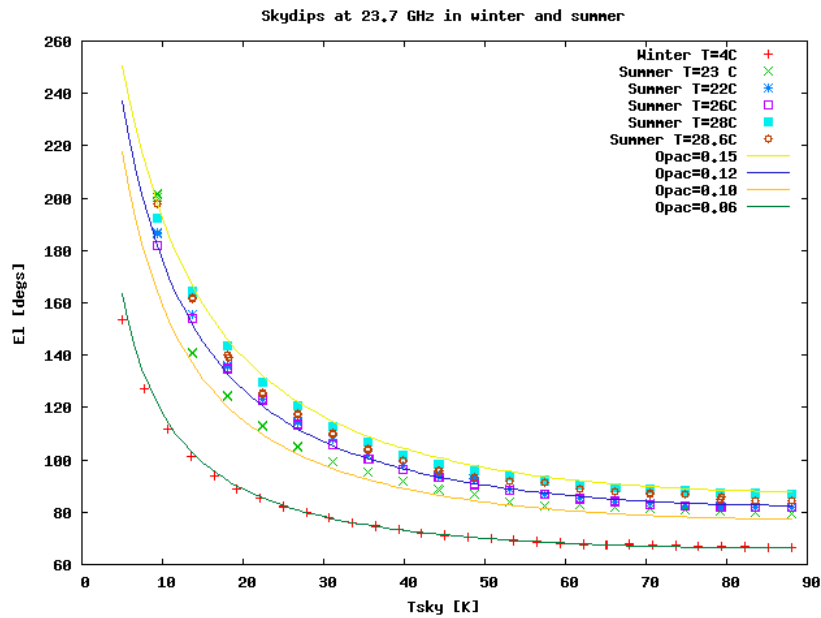


Figure 5: Skydips at 23.7 GHz under several weather conditions. Lower opacity (0.06) is attained in winter and higher opacity (0.15) in summer. Three curves are shown for the same day in summer and opacity in that same day varies between 0.12 and 0.15. Forward efficiency is $\eta_f = 0.93$ and has been computed using all curves.

The values obtained from skydips match approximately those from the estimations obtained from the amount of precipitable water. Further work will be performed in the future by comparing results from skydips and weather conditions at the observatory with a wide variety of weather conditions.

Results from the skydips and estimations of the opacity are summarized in Table 1.

3 Gain curves

Gain curves at 5, 6 and 8 GHz have been determined by tracking DR21 or 3C84 from horizon to zenith. Neither DR21 nor 3C84 are the most intense sources at these frequencies but their flux is high enough to be well above the noise, and both culminate at 88 degrees elevation at Yebes,

Frequency (MHz)	η_f	τ_0 (meas.)	H ₂ O (ATM)	τ_0 (mm)	T _{rec} (K)	Pres. (mbar)	Temp (C)	Hum. (%)	Sky
4900	0.89	0.009	5.8	0.007	71	902.9	0.3	60	Clear
6000	0.91	0.012	5.8	0.007	73	902.9	0.3	60	Clear
6000	0.89	0.012	5.8	0.007	67	902.9	0.3	60	Clear
6600	0.87	0.012	5.8	0.007	82	902.9	0.3	60	Clear
8400	0.85	0.015	4.7	0.008	9	905.7	-0.1	49	Clear
8400	0.85	0.015	14.0	0.008	9	908.9	29.2	25	Clear
22400	0.93	0.06	5.9	0.07	28	915.7	-2.2	70	Clear
22400	0.93	0.17	12.0	0.10	28	914.2	34.0	16	Clear
22400	0.93	0.17	23.0	0.18	28	915.0	23.0	60	Clear
23700	0.93	0.06	12.0	0.08	34	907.3	3.9	95	Clear
23700	0.93	0.12	14.0	0.09	34	907.3	27.0	28	Clear

Table 1: Forward efficiency and zenithal opacity for different sky frequencies obtained from skydips. Water content in the atmosphere, estimated opacity from ATM, receiver temperature (RCP) and weather conditions are included. ATM opacity was computed from a general model for winter/summer at Yebes and the estimated water content in mm.

which allows to obtain the gain at the whole elevation range. Atmospheric opacity effects have not been subtracted since, at these frequencies, the opacity estimated from skydips is lower than 0.02, which would imply a maximum correction of 1.02.

A second order polynomial fit has been performed to the higher values of the available data, since pointing errors yield lower intensity values and should be discarded. The data were normalized to 1.

Maximum gain is attained at 40-45 degrees at 5 and 6 GHz . The gain drops 5 to 10% from the maximum to the minimum in an approximately symmetric curve. At 8 GHz, the behaviour is different: maximum is attained at 30 degrees and the gain drops 30% from the maximum. The minimum happens at elevations close to the zenith and the drop is not symmetric relative to 45 degrees elevation.

Gain curves at 22 GHz have been determined from pointing drifts on 3C84 and DR21. The encoder hysteresis problem (de Vicente 2010) prevents a complete correct pointing model and this generates a high dispersion in the pointing data at different elevations. Since opacity is not negligible, data should be corrected by opacity damping taking into account the zenithal opacity and the airmasses. The assumed zenithal opacity (τ_0) was 0.06 and data should be corrected as follows:

$$T_a^c = T_a e^{\tau_0/\sin(el)} \quad (8)$$

where T_a is the antenna temperature, el elevation and T_a^c the corrected antenna temperature.

If opacity is corrected, the maximum gain at 22 GHz is attained at 10 degrees elevation. The gain drops continuously towards high elevations down to 15%. One might think that this behaviour could come from systematic pointing errors or a systematic defocus of the antenna dependent on elevation. However the pointing error is always below 9 arcsecs (approximately

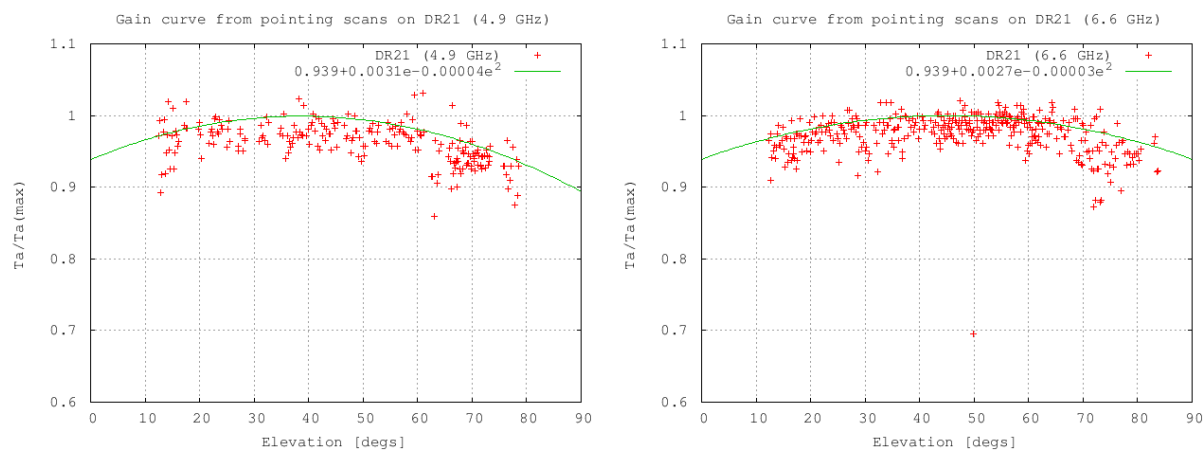


Figure 6: Normalized gain curve obtained from pointing drifts on DR21 at C band. Left: 4.9 GHz, Right: 6.6 GHz

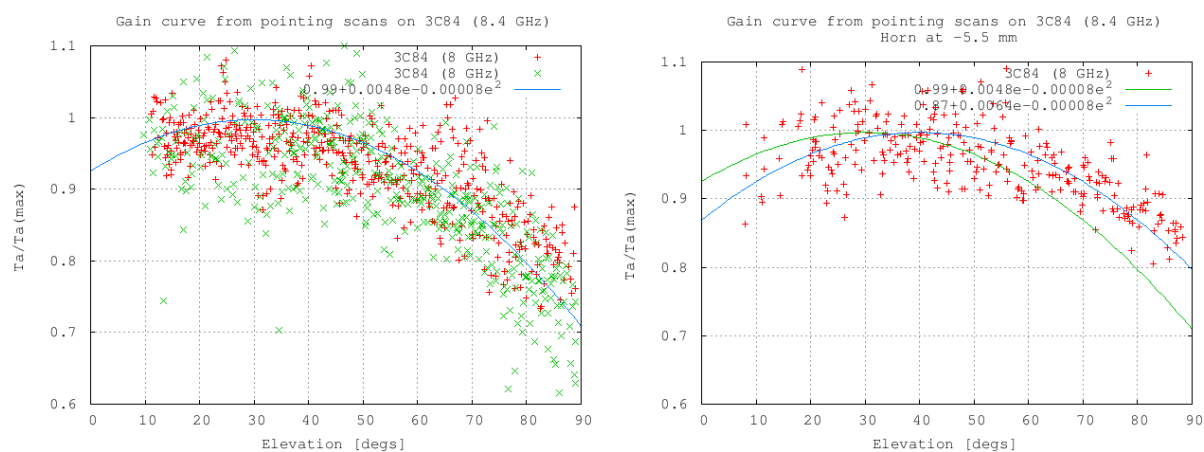


Figure 7: Normalized gain curve obtained from pointing drifts on 3C84 at 8.4 GHz. Left: Horn at 0.0 mm. Right: Horn at -5.5 mm (Updated on Aug. 2010).

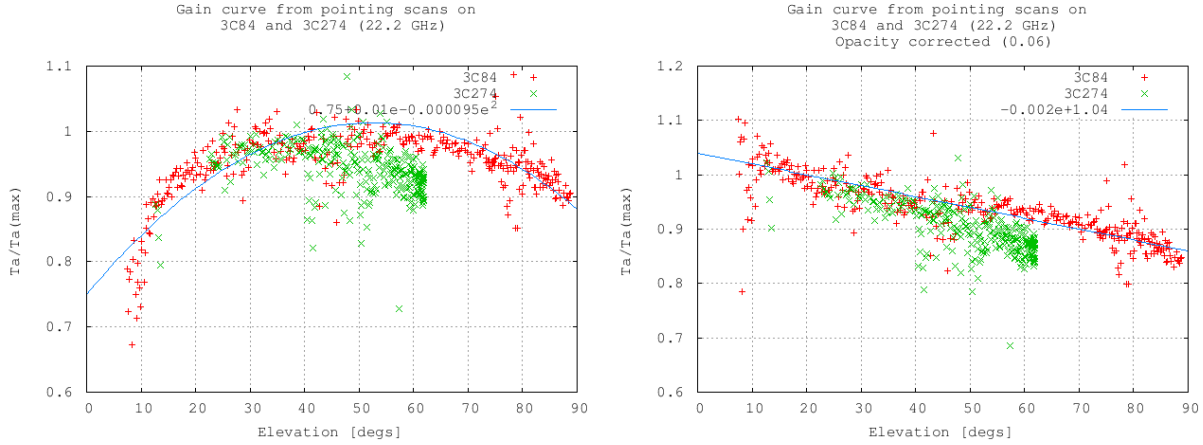


Figure 8: Normalized gain curve obtained from pointing drifts on 3C84 and 3C274 at 22.2 GHz. Left: not corrected by opacity. Right: corrected by atmospheric opacity (zenital opacity of 0.06)

10% of the HPBW), the beamwidth remains constant and close to 80 arcsecs (towards 3C84) and no secondary lobes are seen at different elevations. Fig. 9 shows three pointing drifts at 13, 45 and 86 degrees elevation towards 3C84 to demonstrate the lack of secondary lobes.

In order to estimate the effect of defocusing in the gain we have performed pointing drifts changing the Z focus at 3 different elevations: 50, 60 and 68 degrees on the culmination of 3C273, 3C274 and Venus respectively. Fig. 10 shows the normalized gain as a function of the subreflector displacement. A shift of 2 mm in Z around the best focus causes a gain drop of 5%. Results show that the current focus model seems to be correct because no trend as a function of elevation is seen. Indeed we see a shift in Z opposite at 68 and 60 degrees and no shift at 50 degrees elevation. These variations of ± 2 mm maximum, are probably due to temperature gradients, arising from the difference between day and night and/or direct illumination of the sun on the tetrapod legs or the relative orientation of the antenna with respect to the sun. A systematic 15% drop in gain from 10 degrees elevation to 80 degrees elevation should arise from a systematic defocus with a total displacement of 5 mm at 22 GHz. This effect is not seen in Fig. 10.

A similar measurement was performed for the Y focus at two different elevations towards 3C84. Fig. 10 shows that the normalized gain as a function of Y defocus for two elevation ranges 83-72 degrees and 65-53. These plots should be considered with care. The elevation changes 10 degrees during the whole process and hence the gain also changes. It is rather significant that the gain is higher at any focus around 60 degrees elevation, than at 73 degrees. If the cause of the gain drop were a wrong Y focus, the gain should have been the same at 73 than at 60 degrees at least for one position of the Y focus, and this is not the case.

Our conclusion is that the different gain dependence behaviour as function of frequency probably does not come from a wrong focus setup at X, Y or Z axis. There is no simple explanation for the fact that the maximum efficiency at 6 GHz happens at 45 degrees elevation, at 8 GHz happens at 30 degrees and at 22 GHz happens at 10 degrees, and that the efficiency

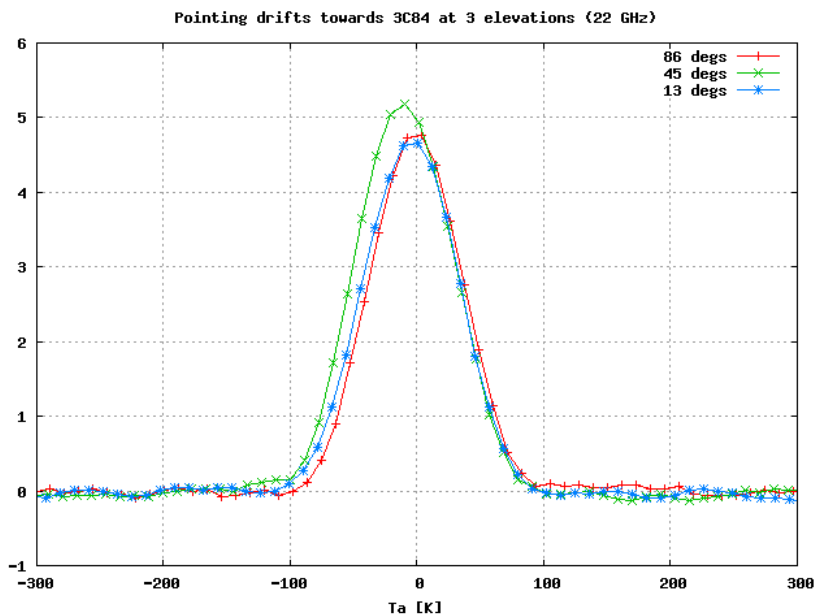


Figure 9: Pointing drifts on 3C84 at 13, 45 and 86 degrees elevation. No secondary lobes, which might indicate defocusing effects, are seen.

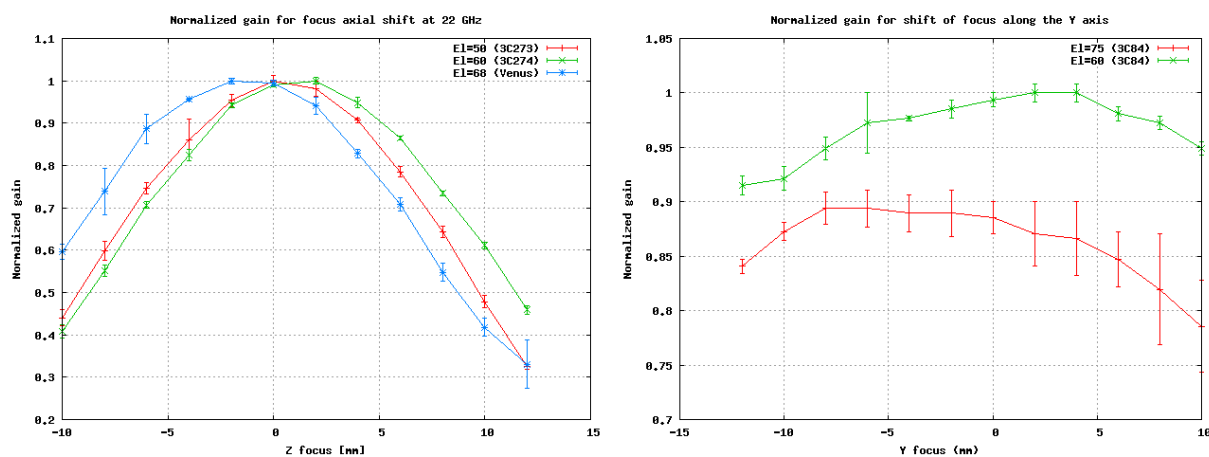


Figure 10: Normalized gain curves obtained from pointing drifts. Left: Z focus shift on 3C84, 3C273 and 3C274 at 22.2 GHz at different elevations. Right: Y focus shift on 3C84 at two different elevation ranges.

a	b	c	Freq. (GHz)
0.939	0.0031	-0.00004	4.9
0.939	0.0027	-0.00003	6.6
0.997	0.0048	-0.00008	8.4
0.87	0.0064	-0.00008	8.4 ⁽¹⁾
0.75	0.01	-9.5 10 ⁻⁵	22.2
1.04	-0.002	0.0	22.2 ⁽²⁾

Table 2: Second order polynomial fit ($a + be + ce^2$) to get a normalized gain curve at different frequencies. (1) horn at -5.5 mm from nominal position. (2) opacity corrected. (Updated August 2010)

drop is maximum at 8 GHz (30%), while it is 15% at 22 GHz and 5% at 6 GHz. Further tests and studies should be performed to find out the causes.

Note (August 1st, 2010): The gain curve at X band improves after shifting the X band horn 5.5 mm along an axis parallel to the elevation axis. Fig. 7b shows the new gain curve obtained by tracking 3C84. A new report will be written with the complete set of measurements and complete details. Some information is already available at de Vicente (2010b)

4 Aperture efficiency, beam efficiency and SEFD

Aperture efficiency has been estimated from pointing drifts on several calibration sources. Table 3 shows a list of sources, their fluxes, antenna temperature and elevation at which the drifts were done.

Source name	5 GHz		6.6 GHz		8 GHz			22 GHz			24 GHz		
	Flux (Jy)	T_a (K)	Flux (Jy)	T_a (K)	Flux (Jy)	T_a (K)	El °	Flux (Jy)	T_a (K)	El °	Flux (Jy)	T_a (K)	El °
3C84		4.0		3.8		5.5		22	4.4	42	27	4.6	49
DR21		4.8		4.2		5.5		21	3.8	42	18	3.4	69
3C454.3	10	2.9	10	2.1	10	3.1	40						
3C123	16	4.2	12	2.6	9.8	3.0	21						
3C274	67	17.2	43	11.1	43	12.5	45	20	3.9	42	19	2.9	12

Table 3: Sources used for estimating the aperture efficiency. Their flux (from VLBA observations in the same epoch) and measured antenna temperature are included at several frequencies. Elevation is only included at 8, 22.4 and 23.7 GHz

Aperture efficiency (η_a) may be computed from the flux and the antenna temperature of a radiosource. According to Baars (1973, 2007):

$$\eta_a = \frac{2K_B T_a}{AS_f C_s} \quad (9)$$

where T_a is the antenna temperature in space (no absorption from the atmosphere), A the radiotelescope collecting area, S_f the source flux and C_s a factor which takes into account the source brightness distribution compared to the antenna HPBW and is only valid for sources whose size is equal or smaller than the beam width:

$$C_s = \begin{cases} 1 + x^2 & \text{gaussian source} \\ \frac{x^2}{1 - \exp(-x^2)} & \text{disk source} \end{cases} \quad (10)$$

where,

$$x = \frac{\theta_s(\prime\prime)}{\theta_b(\prime\prime)} \quad (11)$$

and θ_s is the source size and θ_b the HPBW of the antenna.

Aperture efficiency for point like sources at the 40 m radiotelescope may be approximated by

$$\eta_a = 2.197 \frac{T_a[\text{K}]e^\tau}{S_f[\text{Jy}]} \quad (12)$$

where we have inserted atmospheric opacity at the observed frequency and elevation. This comes from approximating the sources by gaussians in which $\theta_s \ll \theta_b$. Below 8 GHz, opacities are so low that they can be neglected. Opacity at 22 GHz at 90 degrees elevation was approximately 0.09 both frequencies. We have computed the opacity at the elevations at which the sources were observed and corrected the antenna temperature accordingly at 22.2 GHz and 23.7 GHz. Since the antenna temperature depends on elevation, the efficiency also depends on elevation. Estimations in Table 5 have been performed at 45 degrees.

The aperture efficiency is maximum at X band (0.66) and minimum at 6 GHz (0.46). The big difference between the aperture efficiency at 4.9 and at 6.6 GHz is awkward and is probably related to the same effect that causes a discrepancy in the skydips at C band. The aperture efficiency at 4.9 GHz is slightly worse than at X band and we believe that it might be caused by beam truncation. Efficiency at 22 and 23 GHz is almost equal. This small discrepancy may be due to uncertainty in the amplitude calibration or from a poorer determination of the calibration sources at 23.7 GHz. Below we compare these results with predictions from illumination.

Note: August 2010: The aperture efficiency at X band is slightly better after shifting the horn by -5.5 mm. The estimated gain from measurements on 3C274 and 3C123 is $\simeq 0.70$. We have updated Table 5 adding one line for the new horn position.

The beam efficiency is the fraction of all power received which enters the main beam. The main beam is defined to extend to the first null in the radiation pattern. It can be computed for point like sources (Baars 2007) from:

$$\eta_{mb} = \frac{\Omega_m A_g}{\lambda^2} \eta_a \quad (13)$$

$$= \frac{\pi D^2}{4} \frac{1.133}{\lambda^2} \left(\frac{1.16\lambda}{D} \right)^2 = 0.89 1.16^2 \eta_a \quad (14)$$

$$= 1.1976 \eta_a \quad (15)$$

where Ω_m is beam solid angle, A_g the geometrical area, λ the observing length and D the diameter of the antenna.

The main beam efficiency ranges from 0.55 at 6.6 GHz, similar value for 22 GHz, and 0.84 for the X band with the new horn position. At X band the main beam efficiency is almost similar to the forward efficiency and this would mean that, surprisingly, diffraction effects are negligible from the front part of the antenna. This is not the case at the other frequencies. The difference between forward and the main beam efficiency is larger at higher frequencies as expected, since the surface error causes higher diffraction at higher frequency.

Frequency (MHz)	η_a	S_f/T_a (Jy/K)	SEFD (Jy)	η_f	η_{mb}	HPBW
4900	0.60 ± 0.03	3.7 ± 0.2	390 ± 20	0.89	0.72	370 (6.2')
6600	0.46 ± 0.03	4.4 ± 0.2	450 ± 30	0.87	0.55	280 (4.7')
8400	0.66 ± 0.03	3.3 ± 0.2	220 ± 10	0.85	0.79	230 (3.8')
8400 ¹	0.70 ± 0.03	3.2 ± 0.2	210 ± 10	0.85	0.84	230 (3.8')
22400	0.48 ± 0.03	4.6 ± 0.2	296 ± 15	0.93	0.57	75 (1.2')
23400	0.47 ± 0.03	4.7 ± 0.3	332 ± 15	0.93	0.56	75 (1.2')

Table 4: Aperture efficiency at 45 degrees elevation, Jy/K relationship, SEFD, forward and main beam efficiencies and HPBW (in arcsecs and arcminutes). Aperture efficiency, main beam efficiency, Jy/K relationship and SEFD are estimated at 45 degrees elevation at all frequencies and they are opacity (0.09) corrected at 22 GHz and 23 GHz. (1) This line was added on August 2010 and the values were obtained with the new horn position at -5.5 mm.

The SEFD is a measurement of the sensitivity of the telescope that takes into account both the gain of the antenna and the system temperature. It is equivalent to the strength of a hypothetical radio source that results in received power equal to that generated by the receiving system. The lower the SEFD the more sensitive the telescope is. The SEFD is estimated by observing a strong radiource with a known flux S_f :

$$\text{SEFD} = S_f \frac{T_{sys}}{T_a} \quad (16)$$

where T_{sys} is the system temperature and T_a the antenna temperature.

We have computed the SEFD by correcting the antenna temperature by the atmospheric opacity. Results are in Table 5.

It is possible to estimate the main reflector surface error budget by taking into account all factors that have influence on the aperture efficiency: blockage by the legs and the subreflector (η_b), absorption by the membrane at the vertex (η_m), surface errors in the subreflector (η_{m2}) and nasmyth mirrors (η_{nm}), and illumination efficiency (η_i). So we can summarize them as:

$$\eta_a = \eta_{m1}\eta_{m2}\eta_{nm}\eta_{block}\eta_m = \eta_{m1}\eta_x \quad (17)$$

Table 5 summarizes the estimations for each contribution at different frequencies:

The blockage can be estimated from the geometry, see P. de Vicente (1996). Illumination and an estimation of the RMS of the different mirrors was provided by F. Tercero (2009). The

Freq. (GHz)	η_b	η_i	η_m	η_{m2} 50 μm	η_{m3} 25 μm	η_{m4} 25 μm	η_{m5} 80 μm	η_p 50 μm	η_d 50 μm	η_x	η_{m1}
4.9	0.92	0.75	1.0	1.0	1.0	1.0		1.0		0.69	0.87 ± 0.03
6.6	0.92	0.72	1.0	1.0	1.0	1.0		1.0		0.66	0.70 ± 0.03
8.4	0.92	0.75	1.0	1.0	1.0	1.0		1.0	1.0	0.69	0.95 ± 0.03
8.4 ¹	0.92	0.75	1.0	1.0	1.0	1.0		1.0	1.0	0.69	1.01 ± 0.03
22.4	0.92	0.78	0.96	1.0	1.0	0.99	0.99			0.67	0.85 ± 0.03
23.7	0.92	0.78	0.96	1.0	1.0	0.99	0.99			0.67	0.83 ± 0.03

Table 5: Efficiency from the different elements along the radiation path at several frequencies. Last column is the estimated RMS from the efficiency of M1. We have only computed it at 22 GHz since a computation error at lower frequencies has a huge impact in the final figure. (1) This line was added on August 2010 and the estimated η_{m1} was obtained with the new horn position at -5.5 mm.

effect of the membrane can be estimated from models which take into account the dielectric constant of the material and its thickness (Malo 2010).

The best estimate for the RMS error of the main reflector surface can be obtained from the highest frequencies using Ruze's (1966) formula:

$$\sigma_{m1} = \frac{\sqrt{-\ln \eta_{m1}}}{4\pi} \lambda [\mu m] \quad (18)$$

At 8.4 GHz the estimated RMS error is 650 μm , at 22 GHz it is 430 μm and at 23.7 GHz it is 430 μm . The determination of this value should be done at higher frequencies to obtain a better accuracy since these values may show a string variation from a small change in the efficiency of M1 (Fig 11).

Note (August 2010): The new aperture efficiency value for X band yields a value of 1.01 for η_{m1} which cannot be higher than 1. In any case, 1 means that the main reflector has no surface error and obviously this is not the case. However an error of 430 μm , would yield a $\eta_{m1} = 0.98$ which is within the error limits.

5 Beam images

We have made images of the antenna beam at different frequencies to check its shape and look for defocusing and astigmatism effects. This section is a collection of such images on the strongest point like source at each frequency.

5.1 C Band

Figure 12 shows two maps on 3C274 at 4.9 and 6.6 GHz with a maximum simultaneous band of 512 MHz performed on february 18th 2010. The left one was done at 38 degrees, has a size of 3600'' and is sampled with a step of 90 arcsecs, approximately 4 times less than the HPBW. The maximum is 16.3 K and levels start at 0.5 K in steps of 1.58 K. The right map was done at 27

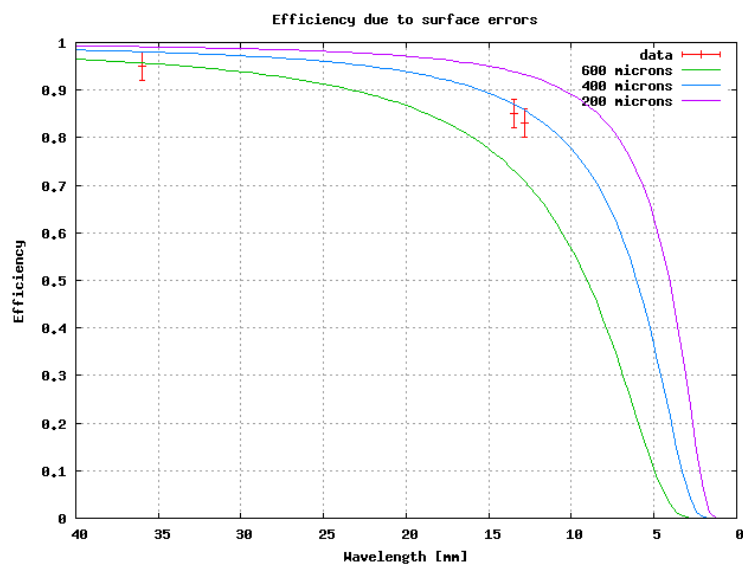


Figure 11: Expected efficiency due to small random surface errors according to Ruze (1966). Three values have been used to show the effect: 600 μm , 400 μm and 200 μm . The values obtained at 3.6 cm (8.4 GHz), 1.35 cm (22.2 GHz) and 1.28 cm (23.4 GHz) have been depicted. The new value for X band would be 0.99 with the same errorbar

degrees elevation, has a size of 2800'' and is sampled with a step of 70 arcsecs (approximately 4 times less than the HPBW). Maximum is 10.68 K and levels start at 0.3 K in steps of 1.03 K.

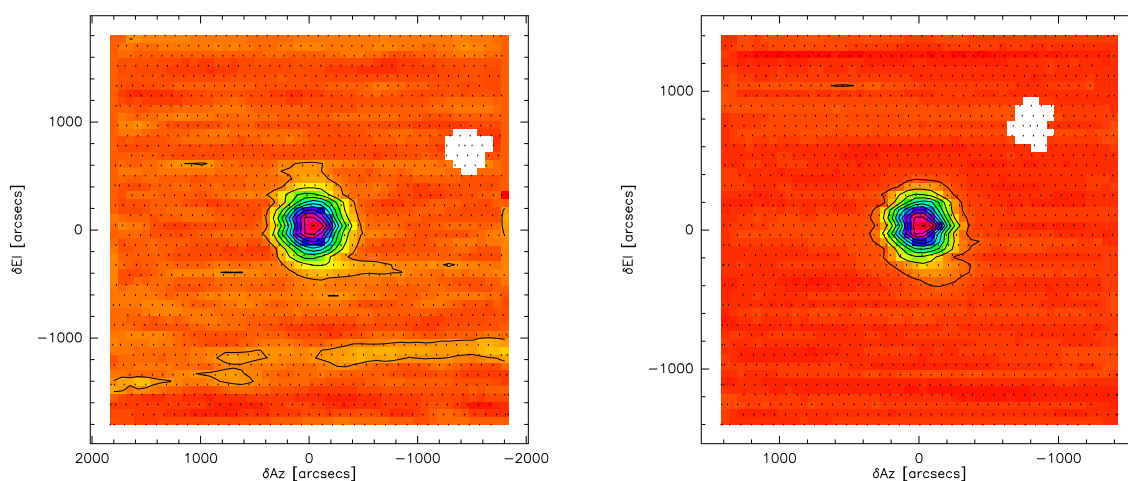


Figure 12: Left panel: Map on 3C274 at 4.9 GHz at 36 degrees elevation. Levels go from 0.5 K to 16.3 K in steps of 1.58 K. Right panel: Map on 3C274 at 6.6 GHz at 27 degrees elevation. Levels go from 0.3 K to 10.68 K in steps of 1.03 K

5.2 X Band

Figure 13 shows a map done on 3C274 at 56 degrees elevation on may 6th 2010 with a maximum simultaneous band of 512 MHz. Maximum is 11.8 K and levels start at 0.5 K in steps of 1.19 K. The lower level is close to the noise. The map has a size of 1800'' and is sampled with a step of 54 arcsecs, approximately 4 times less than the HPBW.

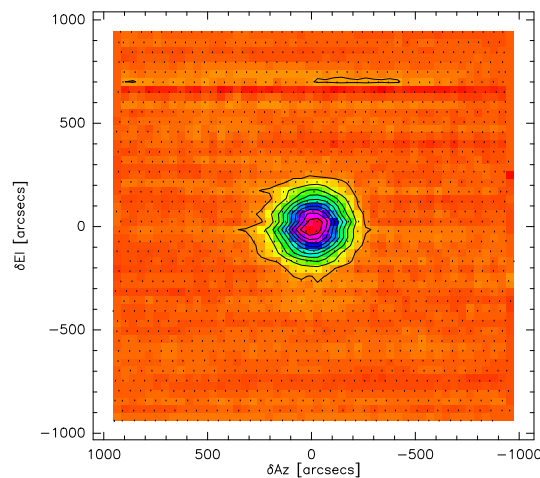


Figure 13: Map on 3C274 at 8.4 GHz. Levels go from 0.5 K to 12.42 K in steps of 1.192 K

5.3 K Band

Figure 14 shows a map done on 3C84 at 40 degrees elevation on february 19th 2010 with a maximum simultaneous band of 512 MHz. Maximum is 5.70 K and levels start at 0.2 K in steps of 0.55 K. Level at 0.1 K has also been depicted to see the trend close to the noise. The lower level is close to the noise. The map has a size of 400'' and is sampled with a step of 10 arcsecs.

5.4 Discussion

The dynamic range is between 20 and 30 for all the previous maps. All show a circular symmetric shape. No obvious elliptical shape, or the presence of secondary lobes are seen in any of the frequencies at this level. The 22 GHz map shows, close to noise level (40 times below the maximum), a trend to get more power along a horizontal axis. This effect could come from astigmatism. If the axial focus is correct, the secondary lobes should be seen 100 times below the maximum. Radio sources used in this report do not allow to have such a large dynamic range.

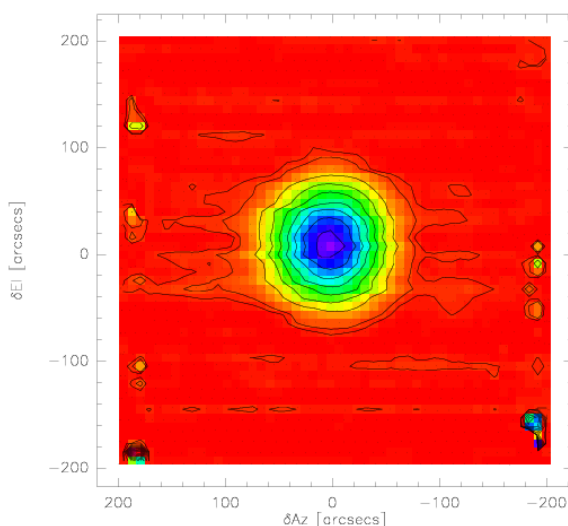


Figure 14: Map on 3C84 at 22 GHz at 40 degrees elevation. Levels go from 0.2 K to 5.70 K in steps of 0.55 K. Level at 0.1 K has also been depicted.

References

- [Baars 1973] J. W. M. Baars. IEEE Trans. Antennas Propag., Vol. AP-21, p. 461 - 474, 1973.
- [Baars 2007] J. W. M. Baars. "The Paraboloidal Reflector Antenna in Radio Astronomy and Communication", Springer 2007.
- [Butler 1998] B. Butler, "Precipitable Water at the VLA – 1990-1998". VLA Scientific Memo No. 176, 1998
- [Clark 1987] B. Clark, "Precision of Meteorological Measurements", VLA Scientific Memo No. 158, 1987
- [de Vicente 1998] P. de Vicente. "Eficiencia por bloqueo en un paraboloide. Antena de 40 m.". Informe Técnico OAN-1998-10.
- [de Vicente 2010a] P. de Vicente, K. Matull, E. Sust, C. Albo. "Encoder hysteresis at the 40m radiotelescope". Informe Técnico OAN-2010-2
- [de Vicente 2010b] P. de Vicente. "Pointing models for the 40 m radiotelescope at 6, 8 and 22 GHz"
- [Malo 2010] I. Malo, J. D. Gallego, M. Diez, I. López, R. García. "Medida de la Permitividad a temperaturas criogénica y ambiente con el método de Perturbación de Cavidad". Informe Técnico OAN-2010-9. 2010

- [Pardo 2001] J. R. Pardo, J. Cernicharo, and E. Serabyn. "Atmospheric Transmission at Microwaves (ATM): An Improved Model for mm/submm applications", *IEEE Trans. on Antennas and Propagation*, 49/12, 1683-1694 (2001)
- [Paine S. 2004] S. Paine, "The am Atmospheric Model", SMA Technical memo 152, 2004.
- [Rozenberg 1966] Rozenberg, G. V. "Twilight: A Study in Atmospheric Optics" (New York: Plenum Press), 1966.
- [Ruze 1966] . J. Ruze. "Antenna Tolerance Theory". *Proc IEEE* 54, 633, 1966.
- [Tercero 2009] . F. Tercero. Private Communication.